




Raman spectra and phonon structures of BaGa₄Se₇ crystal

Yan Yin ^{1,2}✉, Busheng Wang^{1,3}, Yiwen E ^{1,2}, Jiyong Yao⁴✉, Li Wang ¹, Xuedong Bai^{1,2,5} & Wuming Liu^{1,2,5}✉

BaGa₄Se₇ is a promising nonlinear optical crystal at infrared frequencies and shows interesting terahertz phonon-polaritons and high nonlinear coefficients for terahertz generation. Phonons are the key players in infrared absorptions and the photon-phonon resonance phenomena at terahertz frequencies. Here, we study the phonon structures of BaGa₄Se₇ crystal, with polarized Raman spectroscopy and theoretical calculations for phonon dispersion curves, density of states and vibration modes. An interesting phonon gap separates the modes with still or vibrating Ba atoms. We also determine the nine strongest Raman peaks' vibration modes and Raman tensors. Our Raman mode assignments and phonon calculations show consistencies in phonon energies, phonon types, and vibration directions. Above knowledge provides a new case example for phonon gaps, offers a complete picture of the phonon structures of BaGa₄Se₇, and helps us understand phonon gaps, monoclinic crystals, and its phenomena at infrared and terahertz frequency ranges.

¹ Beijing National Laboratory for Condensed Matter Physics and Institute of Physics, Chinese Academy of Sciences, 100190 Beijing, China. ² School of Physical Sciences, University of Chinese Academy of Sciences, 100190 Beijing, China. ³ State Key Laboratory of Metastable Materials Science and Technology & Key Laboratory for Microstructural Material Physics of Hebei Province, School of Science, Yanshan University, 066004 Qinhuangdao, China. ⁴ Technical Institute of Physics and Chemistry, Chinese Academy of Sciences, 100190 Beijing, China. ⁵ Songshan Lake Materials Laboratory, 523808 Dongguan, Guangdong, China. ✉email: yan.yin@iphy.ac.cn; jyao@mail.ipc.ac.cn; wmliu@iphy.ac.cn

Nonlinear optical crystals are the key elements in laser frequency conversions, optical parameter oscillators, and optical signal communications. Particularly, there are needs for better infrared nonlinear optical crystals due to the shortcomings of AgGaQ_2 ($Q = \text{S, Se}$) and ZnGeP_2 ^{1,2}. BaGa_4Se_7 crystal is a promising nonlinear optical crystal working in the infrared region, and exhibits a second harmonic generation about twice of the benchmark material AgGaS_2 ^{3–5}. Phonons are the key players in infrared absorptions, especially in middle and far infrared ranges. In addition, the propagation of terahertz phonon-polaritons⁶ are reported⁷ and high nonlinear coefficients for terahertz generation are observed in BaGa_4Se_7 crystals. Both phenomena are the results of resonances between photons and BaGa_4Se_7 phonons. Therefore, a thorough investigation of the phonon structures of BaGa_4Se_7 is necessary in order to understand its behaviors ranging from infrared to terahertz.

Here, we study the phonon structures of BaGa_4Se_7 crystal, with polarized Raman spectroscopy and theoretical calculations. BaGa_4Se_7 phonon structures show an energy top at about 300 cm^{-1} , which is much smaller than those of most materials. This is consistent with the fact that BaGa_4Se_7 is softer than most materials. The phonon structures also show a phonon gap. This gap separates the modes of still Ba atoms from the modes of moving Ba atoms. Theoretical calculations give the phonon dispersion curves, density of states (DOS) and vibration modes. We determine nine strongest Raman peaks' vibration modes and Raman tensors. Our Raman mode assignments and phonon calculations show consistencies in phonon energies, phonon types, and vibration directions. Above knowledge provides a new case example for phonon gaps, offers a complete picture of the phonon structures of BaGa_4Se_7 , and helps us understand its phenomena at infrared and terahertz frequency ranges.

Results

BaGa_4Se_7 crystal is described by the space group P_c (C_3^2 , group No. 7) of the monoclinic system³. In one of this asymmetric unit cell, there is one unique Ba atom, four unique Ga atoms, and seven unique Se atoms. The irreducible representations classify⁸ the vibration modes of this system into $[2A' + A''] + [34A' + 35A'']$, which are 3 acoustic modes (two A' and one A'') and 69 optical modes ($34A'$ and $35A''$). Due to the low symmetry of this crystal, all those modes are Raman and infrared active. To determine the phonon vibrational configurations and estimate the phonon frequencies, the calculations were carried out within the framework of density functional theory as implemented in the Vienna Ab-initio Simulation Package (VASP)^{9,10}. The exchange or correlation energy was assessed by the generalized gradient approximation in the scheme of Perdew-Burke-Ernzerhof¹¹. The electron-ion interactions were described by means of projector augmented wave¹² with $4s^24p^1$, $4s^24p^4$, and $5s5p6s$ as valence electrons for Ga, Se, and Ba atoms, respectively. We set a $7 \times 7 \times 7$ Monkhorst-Pack¹¹ momentum (k) point mesh and a 500 eV basis set cutoff for the electronic wave functions. Iterative relaxations of cell volume, cell shape, and atomic positions were stopped when the forces generally acting on the atoms were found to be smaller than 0.0001 eV per \AA . With this criterion, the change in the total energy between successive steps was less than 0.01 meV per cell . Phonon calculations were performed using the density functional perturbation theory^{13–15} to get the phonon frequencies and vibration modes at the Γ point. Real-space force constants were calculated within VASP, and phonon frequencies were calculated from the force constants using the PHONOPY code^{16,17}. The resulting phonon dispersion curves and phonon DOS are plotted in Fig. 1 for all 72 modes; the atomic displacements of 9 modes are

shown in Fig. 2 with their type (A' or A'') and their Γ point energies (both from calculations and experiments).

The yellow transparent BaGa_4Se_7 crystals in this study were grown by the Bridgeman method^{4,18}. Three samples were prepared by cutting along different dielectric frame directions (xyz directions in Fig. 2), gave top surfaces with normal directions in x , y , z directions, and were defined as $\langle 100 \rangle$, $\langle 010 \rangle$, $\langle 001 \rangle$ crystals. They have typical size of $13 \times 8 \times 3\text{ mm}^3$ with the thinnest direction in the normal direction. The polarized Raman experiments were performed on a Horiba HR-800 Raman system with a 532 nm excitation laser. The excitation light at the scale of 1 mW were focused on the top surfaces of the samples with a $100\times$, $\text{NA} = 0.9$ objective mounted in a backscattering Raman configuration. Polarized Raman measurements were performed with spectra data named accordingly to the configurations; for instance, xyz spectrum means: the sample is $\langle 100 \rangle$ crystal and its top surface's normal direction is in x direction, the incident light's polarization is in y direction, the analyzer's polarization is in z direction. Twelve configurations were measured at same excitation powers with xyy , xzz , yxx , yyz , zxx , zyy , xyz under 3 s exposure time and xzy , yxz , yzx , zxy , zyx under 20 s exposure time. All the Raman spectra data were analyzed and fitted with multiple Lorentzian peaks to retrieve Raman intensities for individual modes. Figure 3 shows the xyy spectrum and its fitting peaks; other spectra are shown in Supplementary Figs. 1–11; all 12 spectra were processed with the same method as the xyy . Then, the intensities of individual Raman modes from different polarization configurations were combined together (after normalization for different exposure times) to give the Raman tensors. The relative strengths of the elements give the shapes of the Raman tensors, although their absolute strengths are in arbitrary unit. Nine modes' resulting Raman tensors are listed in Table 1, together with the modes' types which are determined from the Raman tensors.

BaGa_4Se_7 's phonon structure. BaGa_4Se_7 's phonon structure shows a relatively low phonon energy cap and a phonon gap. Figure 1a shows the calculated phonon band dispersions along the high-symmetry directions of Brillouin zone for BaGa_4Se_7 . The inset gives the definitions of high-symmetry points in the momentum space. The blue arrows show the momentum path corresponding to the dispersion displayed. The dispersion curves give the maximum phonon energy about 300 cm^{-1} and a phonon gap around 150 cm^{-1} ; both the top of phonon bands and the phonon gap are visible in Raman spectra (see Fig. 3 for example) at corresponding energy locations. We expect the BaGa_4Se_7 crystal is soft and fragile as the result of such a low phonon energy cap. The phonon gap around 150 cm^{-1} is about 45 cm^{-1} wide. Figure 1b shows the phonon DOS for BaGa_4Se_7 . The red, green, and blue shadowed areas are for Ba, Ga, Se atom phonon DOS, respectively. The Ba atom only has phonon distribution within the low energy part just below the phonon gap. It means that the Ba atom doesn't move at all in the phonon modes above the gap. For instance, the 180.8 and 230.5 cm^{-1} modes show no movements of Ba atoms in Fig. 2. All of the upper band phonon modes satisfy the condition of a still Ba atom. The freezing of the Ba atom at upper phonon band probably is due to its place at a high symmetry point of the cell and its heavy weight. Earlier works reported a gap between acoustic and optical phonons in MoS_2 ¹⁹ and WS_2 ²⁰, and phonon gaps in two elements hydrides²¹. Previous reports show that a phonon gap happens in a two-elements crystal with a very heavy atom and a very light atom and with high symmetric conditions. Here, we showed that a phonon gap can happen in a complex three-elements monoclinic crystal, BaGa_4Se_7 , with very low symmetric conditions. Our finding

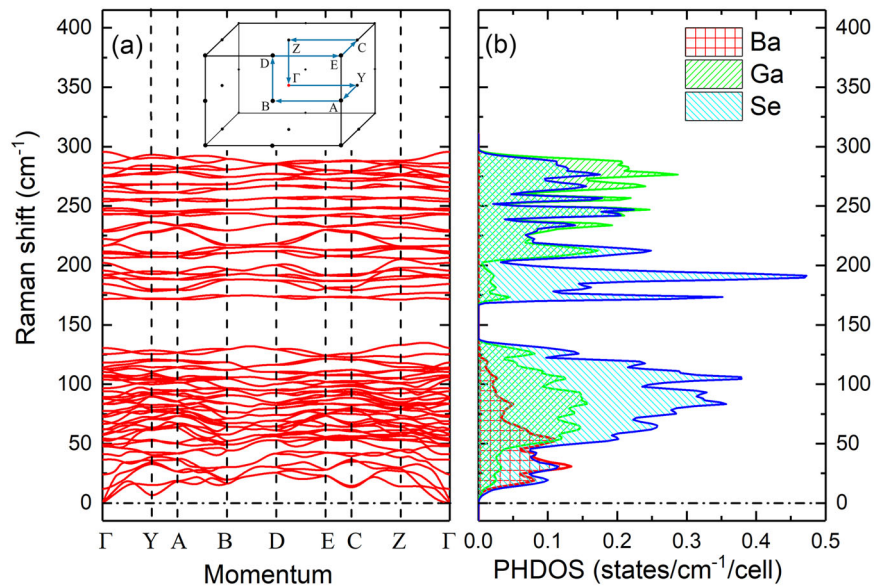


Fig. 1 Calculated phonon dispersions and DOS for BaGa_4Se_7 . **a** Calculated phonon band dispersions along the high-symmetry directions of Brillouin zone for BaGa_4Se_7 . The x axis is the phonon momentum in K space, the y axis shows the phonon energies in units of wavenumbers. The inset gives the definition of high-symmetry points in the momentum space. The blue arrows show the momentum path corresponding to the dispersion displayed. **b** Phonon density of state (PHDOS) for BaGa_4Se_7 . The red, green, and blue shaded areas are for Ba, Ga, Se atom PHDOS, respectively.

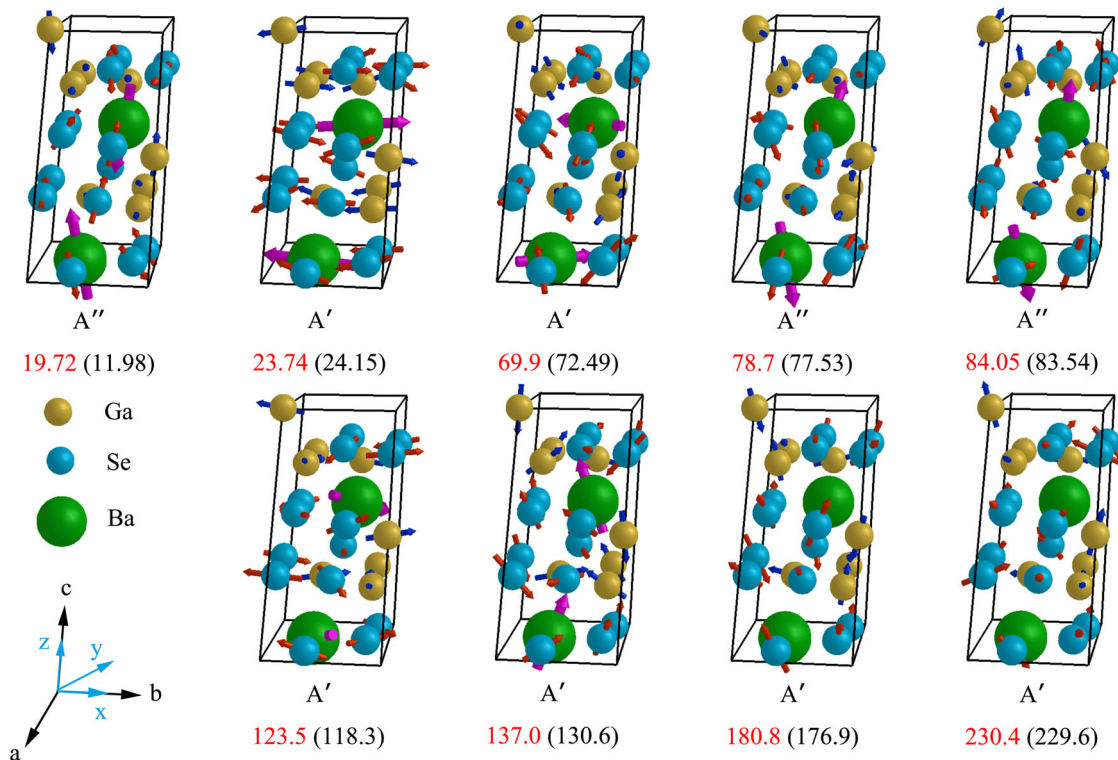


Fig. 2 Main atomic displacements for the optical modes of BaGa_4Se_7 . The Ga, Se, and Ba atoms are denoted by yellow, blue, and green balls; their displacements are indicated by blue, red, and pink arrows, respectively. The axes in the bottom left corner show the crystallographic axes (abc) and the dielectric frames (xyz). Each block with atom locations and displacement arrows shows one mode and total nine modes are listed here. The A' or A'' labels below the blocks indicate the mode symmetries in the C_3^2 group notation. The numbers below the blocks are the experimentally measured (in red) and calculated values (in black) phonon energies.

lowers the requirements for having a phonon gap and suggests that engineering a phonon gap might be achievable in a large amount of different kinds of crystal systems. Also, we feel that the fact, this gap in BaGa_4Se_7 separates the modes with a still or vibrating Ba atom, is interesting and might be potentially useful

for phonon effective mass control and phonon structure engineering. For instance, our calculations show that replacing Ba with a lighter atom, Sr, Ca, or Be will reduce the phonon gap, and replacing Ba with a heavier atom, Ra will enlarge the phonon gap. By engineering two materials with mismatching

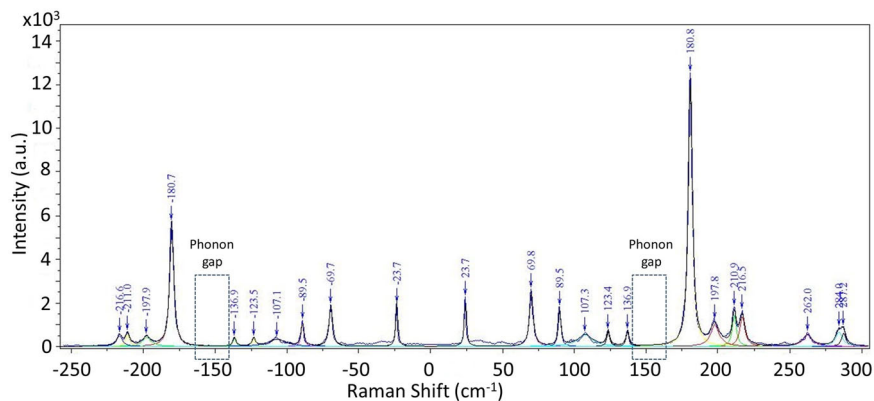


Fig. 3 Raman spectrum and its fitting with multiple Lorentzian peaks of BaGa₄Se₇ under xyy measurement configuration. The center locations of all Lorentzian peaks are listed in the figure. The two dash line rectangles show the locations of the phonon gap, which maintains its positions in the other Raman spectra of different settings.

Table 1 List of nine modes' energies, Raman matrixes and types.

Mode energy (cm ⁻¹)	Average mode energy (cm ⁻¹)	Raman matrix (squares of elements/a.u.)			Type
		<i>yxx, zxx</i>	<i>zyx</i>	<i>yzx</i>	
23.77	23.74	$(30 \pm 2) \times 10^3$	18×10	0 (81)	A'
23.73		37×10	$(53 \pm 9) \times 10^2$	0 (146)	
23.73		0 (81)	0 (145)	$(17 \pm 1) \times 10^2$	
123.65	123.5	$(32 \pm 2) \times 10^3$	16×10	0 (76)	A'
123.36		35×10	$(24 \pm 3) \times 10^2$	0 (103)	
123.38		0 (281)	0	$(26 \pm 1) \times 10^2$	
137.08	137.0	$(105 \pm 2) \times 10^2$	0 (87)	0 (101)	A'
136.89		0 (125)	$(25 \pm 3) \times 10^2$	0 (168)	
137.10		0 (92)	0	$(10 \pm 1) \times 10^3$	
180.79	180.8	$(192 \pm 4) \times 10^2$	0 (704)	0 (331)	A'
180.77		0 (769)	$(63 \pm 5) \times 10^3$	0 (930)	
180.79		0 (288)	0 (539)	$(54 \pm 7) \times 10^3$	
230.4	230.4	$(40 \pm 3) \times 10^2$	0 (26)	0	A'
		0 (30)	0	0	
		0 (67)	0	0	
69.77	69.9	0	669	0 (154)	A'
69.96		644	$(11 \pm 1) \times 10^3$	0	
19.7	19.7	0	0	31×10^2	A''
		0	0	0	
		27×10^2	0	0	
79.06	78.7	0	0	17×10^2	A''
78.36		0 (61)	0	0	
84.0	84.0	14×10^2	0	0	A''
		0	0	0	
		0	0	41×10^2	
		0	41×10^2	0	

The first column shows modes' energies from different polarized Raman setting. The final energies are the averages of the values in column one, are listed in column two. The measured Raman tensors of Stokes modes are listed in the third column. Each component is the square of Raman matrix elements. For components on the diagonal line, the values are the averages of peak fitting results from two diagonal Raman spectra; for other components, the values are single results from one spectrum. For instance, $(30 \pm 2) \times 10^3$, of mode 23.74 cm^{-1} is the average of Stokes Raman peak fitting results from spectra *yxx* and *zxx*, with standard deviation as the error. $(53 \pm 9) \times 10^2$ and $(17 \pm 1) \times 10^2$, are the averages from spectra *xyy* and *zyy*, *yzx*, and *xzz*, respectively. 18×10 is from spectrum *zyx*, and so on. Some component values, for example, 0 (81), are too small compared to the strong values of a same phonon mode, and thus can be neglected as zero with original values in the brackets. Phonon types A' or A'' is determined from the Raman tensor shape and is listed in the fourth column.

phonon gaps, we might have a very large interfacial thermal resistance.

Matching of phonon energies. Our phonon calculations and Raman mode assignments show good coincidence in phonon energies. We list nine modes' atomic displacements in Fig. 2 and their energies, Raman matrixes and types in Table 1. These nine

modes are the strongest modes, and can be identified clearly with matching phonon energies, matching phonon types (A' or A''), and matching main vibration directions between calculations and Raman measurements. In Fig. 2, the Ga, Se, and Ba atoms are denoted by yellow, blue and green balls, whose sizes represent their weights; their displacements are indicated by blue, red and pink arrows, respectively. The axes in the bottom left corner show the crystallographic axes (*abc*) and the dielectric frames (*xyz*), used

in polarized Raman measurements). Each block with atom locations and displacement arrows shows one mode. The numbers below the blocks are the experimentally measured (in red) and calculated (in black) values of phonon energies at Γ point, and they match well between calculations and experiments. We also plotted the experimentally measured (in red) and calculated (in black) values of phonon energies at Γ point of these nine phonon modes, for a comparison, in Supplementary Fig. 12. In Table 1, the first column shows those modes' energies from different polarized Raman setting. Each value is the averages of peak fitting results from two diagonal Raman spectra; only strong spectra and Stokes peaks are used for determining phonon energy for smaller errors. For instance, the first energy value 23.77 cm^{-1} is the average of Stokes Raman peak fitting results from spectra yxx and zxx ; the other two values are the averages from spectra xyy and zyy , yzz , and xzz . The final mode energies are the averages of the values in column one, are listed in column two, and are also shown in Fig. 2 together with calculation values for comparisons. The calculations and experiments show similar values for phonon energies at Γ point.

Phonon types. The phonon type is the second indicator of a good Raman mode assignment. There are only two type of phonons, A' and A'' , in the point group $C_s(m)$ (space group P_c). Their Raman tensors must satisfy $A'(x, y) = \begin{pmatrix} a & d & 0 \\ d & b & 0 \\ 0 & 0 & c \end{pmatrix}$,

$A''(z) = \begin{pmatrix} 0 & 0 & e \\ 0 & 0 & f \\ e & f & 0 \end{pmatrix}$. The A' or A'' labels below the blocks in

Fig. 2 indicate the mode symmetries in the C_3^2 group notation. The phonon types (A' or A'') of those modes are determined independently and are identical, for results both from calculations and experiments. Polarized Raman measurements can give the Raman tensors for modes, thus determine the phonon types. The measured Raman tensors of Stokes modes, for smaller errors, are listed in the third column of Table 1. Each component is the square of Raman matrix elements. For components on the diagonal line, the values are the averages of peak fitting intensity results from two diagonal Raman spectra; for other components, the values are single results from one spectrum. For instance, the first Raman matrix component value, $(30 \pm 2) \times 10^3$, of mode 23.74 cm^{-1} is the average of Stokes Raman peak fitting results from spectra yxx and zxx , with standard deviation as the error. The component values, $(53 \pm 9) \times 10^2$ and $(17 \pm 1) \times 10^2$, are the averages from spectra xyy and zyy , yzz and xzz , respectively. The other component value, 18×10 , is from spectrum zyx , and so on. Some component values are too small compared to the strong component values of a same phonon mode, and thus can be neglected as zero with original small values in the brackets. Because phonon type A' and A'' can only have certain Raman tensor structures, the nine phonon modes' types are determined from their Raman tensor shapes and are listed in the fourth column of Table 1. Both calculations and Raman measurements give identical phonon types for the nine modes.

Matching of vibration directions. In addition, the main vibration direction of each phonon modes matches well between the calculations and Raman measurements. For A' phonons, the main vibration directions are where the strongest components are on the diagonal line of Raman tensors. For instance, the strongest component of mode 23.74 cm^{-1} is $(30 \pm 2) \times 10^3$, and this suggests the main vibration amplitude direction is in x direction. Based on the Raman tensor intensities of those nine modes, the Raman measurements suggest: mode 23.74 , 123.5 , and

230.4 cm^{-1} mainly vibrate in x direction; mode 69.9 cm^{-1} mainly vibrates in y direction; mode 137.0 cm^{-1} mainly vibrates within xz surface; mode 180.8 cm^{-1} mainly vibrates within yz surface. For A'' modes, because only xz or yz elements are non-zero, it seems that the main vibration direction has to be in Z direction due to symmetry conditions. In Fig. 2, calculations show atomic displacements of those modes with color arrows; they are indeed mainly in the directions as Raman tensors suggest. For instance, mode 23.74 cm^{-1} in the second block of Fig. 2 clearly shows mostly vibrating in the x direction. So, the theoretical calculations are in consistence with the experimental findings, not only in phonon energies and phonon types but also in vibration directions.

In terms of Raman mode intensities, the 180.8 cm^{-1} mode is the outstanding and strongest Raman peak (see Fig. 3). This is also supported by the strongest Raman tensor values, 6×10^4 in yy setting and 5×10^4 in zz setting, which are about twice of the largest values of other modes. The strong intensity of the 180.8 cm^{-1} mode partly is benefitted from its largest phonon density of states, which shows up as the strongest peak in the Fig. 1b. The rest of Raman peaks in the spectra are much weaker than the 180.8 cm^{-1} mode.

Discussion

As a promising nonlinear optical crystal in the infrared region, BaGa_4Se_7 also shows phonon strongly related polariton dynamics with terahertz waves and high nonlinear coefficients for terahertz generation due to phonon resonances. In this work, we studied the phonon structures of BaGa_4Se_7 crystal, with both polarized Raman spectroscopy and theoretical calculations. Theoretical calculations present the phonon dispersion curves, DOS, and vibration modes. Our Raman mode assignments and phonon calculations show consistencies in phonon energies, phonon types, and vibration directions. We also listed nine strongest Raman peaks' vibration mode pictures and Raman tensors. Above detailed phonon information will greatly help us to understand BaGa_4Se_7 's behaviors at terahertz and infrared frequency ranges. In addition, an interesting phonon gap appears in this three-elements monoclinic crystal and separates modes with a still or vibrating Ba atom. This might be potentially useful for phonon effective mass control and phonon structure engineering. For instance, by engineering two materials with mismatching phonon gaps, we might have a very large interfacial thermal resistance. Overall, this study of BaGa_4Se_7 phonon structures will help us understand phonon gaps, monoclinic crystals, and BaGa_4Se_7 's interactions with infrared and terahertz frequency light.

Data availability

The data that support the findings of this study are available from the corresponding author upon reasonable request.

Received: 28 August 2019; Accepted: 23 January 2020;

Published online: 11 February 2020

References

- Zawilski, K. T., Schunemann, P. G., Setzler, S. D. & Pollak, T. M. Large aperture single crystal ZnGeP_2 for high-energy applications. *J. Cryst. Growth* **310**, 1891–1896 (2008).
- Isaenko, L., Vasilyeva, I., Merkulov, A., Yeliseyev, A. & Lobanov, S. Growth of new nonlinear crystals LiMX_2 ($M = \text{Al, In, Ga}$; $X = \text{S, Se, Te}$) for the mid-IR optics. *J. Cryst. Growth* **275**, 217–223 (2005).
- Yao, J. Y. et al. BaGa_4Se_7 : a new congruent-melting IR nonlinear optical material. *Inorg. Chem.* **49**, 9212–9216 (2010).

4. Yao, J. Y. et al. Growth and characterization of BaGa4Se7 crystal. *J. Cryst. Growth* **346**, 1–4 (2012).
5. Yang, F. et al. High efficiency and high peak power picosecond mid-infrared optical parametric amplifier based on BaGa4Se7 crystal. *Opt. Lett.* **38**, 3903–3905 (2013).
6. Stoyanov, N. S., Ward, D. W., Feurer, T. & Nelson, K. A. Terahertz polariton propagation in patterned materials. *Nat. Mater.* **1**, 95–98 (2002).
7. E, Y., Yao, J. Y. & Wang, L. Propagation of terahertz waves in a monoclinic crystal BaGa4Se7. *Sci. Rep.* **8**, 16229 (2018).
8. Kroumova, E. et al. Bilbao crystallographic server: useful databases and tools for phase-transition studies. *Phase Transit.* **76**, 155–170 (2003).
9. Kresse, G. & Furthmuller, J. Efficiency of ab-initio total energy calculations for metals and semiconductors using a plane-wave basis set. *Comput. Mater. Sci.* **6**, 15–50 (1996).
10. Kresse, G. & Furthmuller, J. Efficient iterative schemes for ab initio total-energy calculations using a plane-wave basis set. *Phys. Rev. B* **54**, 11169–11186 (1996).
11. Perdew, J. P., Burke, K. & Ernzerhof, M. Generalized gradient approximation made simple. *Phys. Rev. Lett.* **77**, 3865–3868 (1996).
12. Kresse, G. & Joubert, D. From ultrasoft pseudopotentials to the projector augmented-wave method. *Phys. Rev. B* **59**, 1758–1775 (1999).
13. Baroni, S., Giannozzi, P. & Testa, A. Green-function approach to linear response in solids. *Phys. Rev. Lett.* **58**, 1861–1864 (1987).
14. Baroni, S., de Gironcoli, S., Dal Corso, A. & Giannozzi, P. Phonons and related crystal properties from density-functional perturbation theory. *Rev. Mod. Phys.* **73**, 515–562 (2001).
15. Gonze, X. Adiabatic density-functional perturbation-theory. *Phys. Rev. A* **52**, 1096–1114 (1995).
16. Togo, A., Oba, F. & Tanaka, I. First-principles calculations of the ferroelastic transition between rutile-type and CaCl₂-type SiO₂ at high pressures. *Phys. Rev. B* **78**, 134106 (2008).
17. Togo, A., Chaput, L., Tanaka, I. & Hug, G. First-principles phonon calculations of thermal expansion in Ti₃SiC₂, Ti₃AlC₂, and Ti₃GeC₂. *Phys. Rev. B* **81**, 174301 (2010).
18. Guo, Y. W. et al. Synthesis, growth of crack-free large-size BaGa4Se7 crystal, and annealing studies. *Cryst. Growth Des.* **19**, 1282–1287 (2019).
19. Jiang, J. W. Phonon bandgap engineering of strained monolayer MoS₂. *Nanoscale* **6**, 8326–8333 (2014).
20. Berkdemir, A. et al. Identification of individual and few layers of WS₂ using Raman spectroscopy. *Sci. Rep.* **3**, 1755 (2013).
21. Fu, Y. H. et al. High-pressure phase stability and superconductivity of pnictogen hydrides and chemical trends for compressed hydrides. *Chem. Mater.* **28**, 1746–1755 (2016).

Acknowledgements

This work was supported by the National Key R&D Program of China (Grants No. 2016YFA0301500), the National Natural Science Foundation of China (Grant No.

11574388, 61775233, 11434015, 61835013), and the Strategic Priority Research Program of the Chinese Academy of Sciences (Grants No. XDB01020300, XDB21030300). Yan Yin thanks Prof. Pingheng Tan for providing instruments for the Raman measurements and Prof. Yulong Liu for helpful discussions.

Author contributions

Y.Y. created and coordinated the project, designed experiments, performed data analysis, and wrote the manuscript with the contributions from other authors; B.W. and W.L. performed theoretical calculations; Y.E. performed Raman experiments; J.Y. provided BGSe samples, X.B., L.W., and W.L. provided funding support, guidance, and discussions. All authors reviewed the results and edited and approved the final version of the manuscript.

Competing interests

The authors declare no competing interests.

Additional information

Supplementary information is available for this paper at <https://doi.org/10.1038/s42005-020-0302-x>.

Correspondence and requests for materials should be addressed to Y.Y., J.Y. or W.L.

Reprints and permission information is available at <http://www.nature.com/reprints>

Publisher's note Springer Nature remains neutral with regard to jurisdictional claims in published maps and institutional affiliations.



Open Access This article is licensed under a Creative Commons Attribution 4.0 International License, which permits use, sharing, adaptation, distribution and reproduction in any medium or format, as long as you give appropriate credit to the original author(s) and the source, provide a link to the Creative Commons license, and indicate if changes were made. The images or other third party material in this article are included in the article's Creative Commons license, unless indicated otherwise in a credit line to the material. If material is not included in the article's Creative Commons license and your intended use is not permitted by statutory regulation or exceeds the permitted use, you will need to obtain permission directly from the copyright holder. To view a copy of this license, visit <http://creativecommons.org/licenses/by/4.0/>.

© The Author(s) 2020